Effectiveness of different biochar in aqueous zinc removal

Hien, Nguyen Van; Valsami-Jones, Eva; Vihn, Nguyen Cong; Phu, Tong Thi; Tam, Nguyen Thi Thanh; Lynch, Iseult

DOI:
10.1016/j.biteb.2020.100466

Document Version
Publisher's PDF, also known as Version of record

Citation for published version (Harvard):
Hien, NV, Valsami-Jones, E, Vihn, NC, Phu, TT, Tam, NTT & Lynch, I 2020, 'Effectiveness of different biochar in aqueous zinc removal: correlation with physicochemical characteristics', *Bioresource Technology Reports*, vol. 11, no. 100466, 100466. https://doi.org/10.1016/j.biteb.2020.100466

Bioresource Technology Reports 11 (2020) 100466

Contents lists available at ScienceDirect

Bioresource Technology Reports

journal homepage: www.journals.elsevier.com/bioresource-technology-reports

Effectiveness of different biochar in aqueous zinc removal: Correlation with physicochemical characteristics

Nguyen Van Hien[a,b], Eugenia Valsami-Jones[a], Nguyen Cong Vinh[b], Tong Thi Phu[b], Nguyen Thi Thanh Tam[b], Iseult Lynch[a,*]

[a] School of Geography, Earth and Environmental Sciences, University of Birmingham, Edgbaston, B15 2TT, United Kingdom
[b] Department of Land Use, Soils and Fertilizers Research Institute, Hanoi, Viet Nam

ARTICLE INFO

Keywords:
Characterization
Adsorption isotherm
Functional groups
Inorganic groups
Adsorption mechanism

ABSTRACT

Bochar from typical Vietnamese biomass residues (acacia wood chip, rice husk, bamboo) were assessed for application in remediation of metal-contaminated water. The biochar physical (e.g., surface area, morphology) and chemical (e.g. surface functional groups, proximate and elemental analysis) characteristics were correlated with their effectiveness in removing zinc (Zn^{2+}). The impact of biochar dose, contact time, and initial adsorbate concentration were investigated to determine the adsorption capacity of the biochar for Zn^{2+}. All three effectively remove Zn^{2+} from aqueous solution, with bamboo biochar especially efficient (removal of 96–98% Zn^{2+} from 40 to 80 mg/L). Maximum adsorptions were 7.62, 4.02, and 3.82 mg Zn^{2+}/L for bamboo, wood, and rice husk biochar, respectively. The Freundlich model fit the adsorption of Zn^{2+}, and a pseudo-second order model described the adsorption kinetics. Adsorption was governed by chelation with biochar organic groups (-COOH, $-OH^-$) and precipitation onto inorganic groups (CO_3^{2-}, PO_4^{2-}), not ion exchange.

1. Introduction

Biochar (BC) is the carbonized product gained by pyrolysis of biomass under restricted or absent oxygen conditions (Mukherjee and Zimmerman, 2013) but without an activation step, and thus differs from activated carbon (Qiu et al., 2009). The justification for carbonization through pyrolysis is to avoid the negative influences on human health and the environment that result from direct (in field) burning of biomass residues which releases carbon dioxide, one of the most important greenhouse gases (Al-Wabel et al., 2013). Biomass-derived biochar is formed via a complex process but the reaction mechanism of biomass pyrolysis can be described as occurring mainly via three steps (Demirbas, 2004). The first step is loss of moisture from the biomass, which becomes dry feedstock by heating. Then pre-biochar and volatile compounds are formed. In the last step, chemical compounds in the biosolid rearrange and form a carbon-rich solid product, known as biochar. The volatiles are either condensable such as bio-oil, or non-condensable gases known as syngas, including hydrogen (50%), carbon dioxides (30%), nitrogen (5%), methane (5%), and others (Sohi et al., 2009). As a result of its aromatic structure, biochar can be recalcitrant to microbial decomposition and mineralization, which leads to its persistence in soil for hundreds of years (Zheng et al., 2010).

Pyrolysis conditions impact on the physicochemical characteristics of the resulting biochar. For example, the ash content, pH, and BET surface area increased, while cationic exchange capacity (CEC), volatile matter and micropore (defined as pores < 2 nm in diameter) area declined in biochar produced from sewage sludge at 600 °C compared to biochar prepared at 400 °C (Méndez et al., 2013). On the other hand, a dramatic increase from 0.007 m^2/g to 274 m^2/g in micropore area was observed for biochar derived from Cottonseed hull when the pyrolysis temperature increased from 650 °C to 800 °C (Uchimiya et al., 2011). Losses in total N, organic carbon (OC), and CEC were also found in poultry litter biochar when the pyrolysis temperature rose from 300 °C to 600 °C, while the opposite trend was seen for pH and BET surface area (Song and Guo, 2012). Similarly, at low temperature (< 300 °C), compounds containing -OH, aliphatic C−O and ester C═O groups were removed from the outer surface, while volatile matter shielding or connecting to aromatic cores were destroyed or partly emitted at higher temperatures (> 300 °C) (Mukherjee et al., 2011). Thus, micropores dominating the biochar surface are filled by volatile compounds, which are emitted during pyrolysis as the temperature increases, dramatically enlarging the surface area of the resulting biochar (Cheng et al., 2008).

The biomass materials used for biochar production also have a major influence on the resulting biochar properties. For instance, wood

* Corresponding author.
E-mail address: i.lynch@bham.ac.uk (I. Lynch).

https://doi.org/10.1016/j.biteb.2020.100466
Received 23 February 2020; Received in revised form 27 May 2020; Accepted 27 May 2020
Available online 30 May 2020

and grass biomass-derived biochar normally contain low nutrient elements, in part due to emissions of nitrogen during the pyrolysis process, so the resulting biochar has much lower N content than bichar produced from fertilizers (Cantrell et al., 2012). Biochar formed from waste wheat straw and tree leaves contained higher organic carbon (OC) content (64%–73.9%) than that of poultry litter-derived biochar (36.10%) produced at the same temperature (400 °C) (Song and Guo, 2012). In addition, different biomass sources affect the morphology of the resulting biochar; for instance, the exoskeleton of tracheids (elongated cells in the xylem of vascular plants that serve in the transport of water and mineral salts) was an important contributor to the structure of wood biochar, while a heterogeneous structure resulted from chicken manure biochar (Joseph et al., 2010). The CEC and pH of poultry litter-produced biochar were observed to be higher than those of pine chip biochar and peanut hull biochar (Gaskin et al., 2008).

Biochar (BC) produced from different feedstocks also have a variety of different adsorption capacities and indeed absorption mechanisms. Complexation and precipitation governed heavy metal adsorption to pig and cow manure-derived biochar whose adsorption capacity (q_e) was 50.42–80.88 mg/g for Zn^{2+}; 74.95–94.71 mg/g for Cu^{2+}; 79.55–122.11 mg/g for Cd^{2+}, and 153.76–229.98 mg/g for Pb^{2+} (Kołodyńska et al., 2012). Lower adsorption capacity was observed for Zn^{2+} and Cu^{2+} (6.79 and 4.54 mg/g respectively) for hard wood BC and 12.52 and 11.0 mg/g respectively for corn straw BCs (Chen et al., 2011), while the biochar produced from beech wood chips and garden green waste residues adsorbed only 0.97–2.23 mg/g Zn^{2+}, 1.99–7.80 mg/g Cd^{2+}, and 2.5–3.65 mg/g Cu^{2+} (Frišták et al., 2015). Although the different biochar had different adsorption capacities, their experimental data were well fitted by the Langmuir model, which means that the adsorption resulted in formation of a monolayer on a homogenous surface. In contrast, optimal fitting with the Freundlich model was observed for Scots pine and Silver birch BC (produced at both 450 °C and 700 °C) (Mubarak et al., 2013), and for biochar produced from sugarcane bagasse, eucalyptus forest residues, castor meal, green pericarp of coconut, and water hyacinth (Doumer et al., 2016).

Contamination of aqueous environments by inorganic pollutants is a considerable concern for many countries. Pollution is especially prevalent in developing countries where wastewater and solid waste treatments or recycling are limited due to the lack of affordable treatment technologies and suitable management processes. The presence of heavy metals in the environment leads to toxicity to aqueous flora and fauna, and may cause impacts to human health via the food chain. Metal elements having atomic weights in the range 63.5–200.6 g/mol (or Daltons) and having a specific gravity higher than 5.0 are called heavy metals. One such metal that has attracted significant research interest is zinc (Zn), because both plants and humans require some Zn for growth, but too much is extremely toxic. The most important role of Zn in both plants and humans is related to the activities of several enzymes (Dali-Youcef et al., 2006; Kabata-Pendias, 2010). However, excess Zn in humans leads to toxicity and physiological effects such as vomiting, dehydration, electrolyte imbalance, abdominal pain, nausea, lethargy, dizziness and lack of muscular coordination (Dali-Youcef et al., 2006), while in plants the consequences of excess Zn include decreased growth and chlorosis (loss of their green colour from leaves) (Kabata-Pendias, 2010). Hence, the acceptable level of Zn in drinking water is limited to 3 mg/L (OECD, 2004) to ensure that sufficient is available to meet the bodily needs, but that there is no risk of accumulation and toxicity.

The sources of Zn release into wastewater or soil environments are mainly from industrial activities such as steel production or mining activities (Kabata-Pendias, 2010). Several technologies have been developed to control or remove heavy metals and other pollutants before they are discharged into the environment, including chemical precipitation (González-Muñoz et al., 2006), ion exchange (Doula, 2009), membrane filtration (Samper et al., 2009), and adsorption (Kabbani et al., 2014). Among these methods, the latter is now known as a potential approach for the removal of heavy metals using various adsorbents such as activated carbon (Moreno-Barbosa et al., 2013), carbon nanotubes (Lu and Chiu, 2006), and biochar (Beesley and Marmiroli, 2011). However, activated carbon and carbon nanotubes are costly for application, so low–cost products such as biochar bring advantages especially for developing countries such as Vietnam, enabling repurposing of agricultural waste that would otherwise be burned in fields.

The objective of this study was to investigate the adsorption capacity for Zn^{2+} cations, as a representative aquatic heavy metal pollutant, of different Vietnamese biochar, as representative of biochar produced in developing countries. The biochar were derived from acacia wood, rice husk, and bamboo biomass and were generated using a locally developed top-lid updraft drum approach and were tested using aqueous Zn solutions with the aim to correlate the absorption behaviour with the physical and chemical characteristics of the biochar in order to determine function-activity relationships. The hypothesis being addressed in the study is that the different surface chemistries, surface areas and morphological characteristics of the biochar from different agricultural residue biomass would lead to different adsorption efficiencies, allowing subsequent selection by farmers of the biochar with optimal functionality. In addition, there is significant discussion in the literature as to whether Zn^{2+} adsorption onto biochar occurs via homogenous and/or heterogeneous processes and as a monolayer and/or multilayer, and indeed this may be dependent on the specific features of the biochar and its originating biomass. Thus, this work also aims to determine the mechanisms of adsorption onto the different Vietnamese biochar and thus add to the knowledge base for subsequent development of predictive models.

2. Materials and methodology

2.1. Biochar preparation

2.1.1. Materials for biochar production

The biomass residues used for biochar production in this study were collected from small processing factories in a suburb of Hanoi city. The feedstocks include acacia wood chip, rice husk and bamboo. The wood and bamboo were chopped into suitable pieces to fit into the Top-Lid Updraft Drum (TLUD) equipment and sun-dried before the pyrolysis process. The moisture content of the wood chip, rice husk and bamboo were 14.69 ± 0.47%, 11.58 ± 0.57%, and 14.58 ± 55%, respectively, post sun-drying. The TLUD was used to produce the three biochar from acacia wood chip, rice husk, and bamboo under limited oxygen conditions at a temperature around 550 °C. The TLUD technology consists of a barrel (208.19 L, height 0.87 m, diameter 0.58 m with a chimney) which is described in detail in Fig. 1, and has been used in several previous biochar studies (Joseph and Taylor, 2014; Vinh et al., 2014). The three different biochar were produced simultaneously in a TLUD that has been modified to allow the use of various feedstocks in parallel, resulting in biochar produced under identical conditions. The materials are put into the drum in parallel layers of about 20 cm thickness to ensure uniformity in temperature for each feedstock. Each feedstock layer was packed tightly and compressed before the next layer was added. The final layer is wood, as wood stays alight (wood-embers) for a long time, and thus is used to reduce the smoke formed during the pyrolysis process. A fire is started at the top of the material (wood) and then the lid and chimney are placed on top, once a flame is established. When the fire moved to the haft of the drum, all the holes in the middle and at the bottom were closed and only the 16 holes with d = 5 cm (see Fig. 1) were opened to supply oxygen. When the holes closed, the flame is damped and “biochar” starts to form under limited oxygen. After the biochar started to form, 1 L of deionized (DI) water was injected inside the drum via the 16 holes (d = 5 cm) row in order to maintain a temperature around 550 °C. The total process takes about 3 h, after which the lid is removed and water is sprayed inside the drum

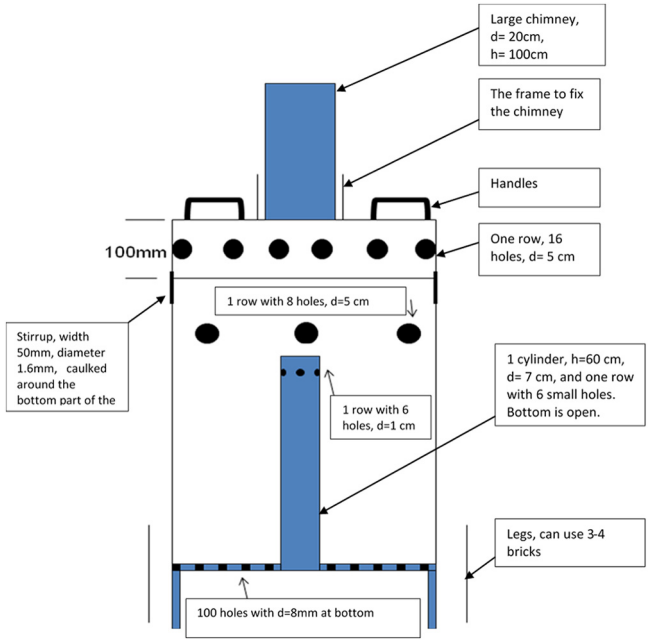

Fig. 1. Modified TLUD for biochar production.

to extinguish the fire and cool the product. Upon cooling, the layers of biochar can be removed and separated. After that, 1 kg of each biochar from wood (WBC), rice husk (RBC), and bamboo (BBC) biomass was stored in air tight plastic bags and shipped to the University of Birmingham, UK. The samples were kept at room temperature in the lab for analysis.

2.2. Biochar characterization

The samples were characterized through BET surface area, Scanning Electron Microscopy (SEM), Fourier transform infrared spectroscopy (FTIR), elemental and proximate analysis, and CEC.

2.2.1. pH_{H2O} analysis

Biochar, sieved through a 2 mm mesh, were analyzed for pH using the method of (Rajkovich et al., 2012). Briefly, distilled water, with ratio of biochar to DI water of 1:25 (w/v), was added to the biochar and the solvent was shaken for 1.5 h to ensure good contact between the water and the biochar's internal surface. Then, the solvent was stirred again by steel spatula and the pH of the solvent was continuously measured using a Thermo Orion 3 star pH meter.

2.2.2. Cation exchange capacity (CEC)

CEC was determined using the method described in (Rajkovich et al., 2012). In brief, 1.0 g of the biochar sieved through a 2 mm mesh was saturated with 50 mL of 1 N CH_3COONH_4 (pH = 7) and the mixture solution was shaken on a shaker table overnight which ensured that the biochar surfaces were sufficiently wetted. After shaking, the solution was filtered by vacuum filter (0.22 μm) and then 40 mL of 1 N CH_3COONH_4 was added and immediately extracted by filtration. Next, 60 mL of ethanol (80%) was used to wash all unbound NH_4^+ from around the samples. The biochar samples were placed into a glass beaker and 50 mL of 1 N KCl was added. The solutions were kept for 16 h in order to reach equilibrium during which time the NH_4^+ absorbed to the biochar was completely replaced by K^+, then immediately another 40 mL of 1 N KCl was added for a subsequent extraction. The solutions containing NH_4^+ which was replaced by K^+ were quantified by Ion Chromatography (Dionex DX500) using 6 standards (0, 0.5, 1.0, 5.0, 10.0, 20.0, 50.0 mg/L of NH_4^+).

2.2.3. Scanning electron microscopy (SEM)

Small pieces of initial biochar were selected and further dried at 60 °C in an oven overnight. Then, 4–5 small pieces of each biochar sample were coated with 10 nm Au/Pt film using a Cressington SC7640 sputter coater and kept in a desiccator overnight. A scanning electron microscope (Philips ESEM XL30 FEG model) operating at accelerating voltages of 10–20 kV was used to image the biochar.

2.2.4. BET surface area

Surface area was determined by the Brunauer, Emmett, and Teller (BET) method. The method is based on Langmuir's theory for monolayer molecular adsorption to multilayer adsorption with the hypotheses that physical adsorption of gas molecules onto a solid occurs in layers, with no interaction between each adsorption layer. A Surface Area Analyzer (model SA 3100) was used for this analysis. Approximately 1 g of biochar (adsorbent), sieved through a 2 mm mesh, was loaded into the vessel. Prior to the determination of the adsorption isotherm, outgassing was conducted to remove the physically adsorbed substances from the adsorbent at 250 °C for 3 h. After degassing was complete, the sample vessel was weighed to determine exactly the weight of the adsorbent, which was used for BET surface analysis. Then, nitrogen gas (adsorbate) was admitted into the sample vessel at cryogenic temperature by the gas adsorption technique. The pressure in the sample vessels was measured for each volume of the gas added until the adsorbate and adsorbent are in equilibrium. The surface area of the samples was measured by plotting the data as a straight line with $y = 1/v[(P/P_0)-1]$ and $x = P/P_0$ following Eqs. (1) & (2) (Brunauer et al., 1938).

$$\frac{1}{V\left[\left(\frac{P_0}{P}\right)-1\right]} = \frac{C-1}{V_m C}\left(\frac{P}{P_0}\right) + \frac{1}{V_m C} \tag{1}$$

where P_0 and P are the equilibrium and the saturation pressure of the adsorbate, V is the volume of adsorbed gas, and V_m is the volume of the monolayer-adsorbed gas, C is the BET constant, and:

$$C = \exp\left(\frac{E_1 - E_l}{RT}\right) \tag{2}$$

where E_1 and E_l represent the heat of adsorption for the first and higher layers, respectively. A total surface area $S_{BET,total}$ and a specific surface area S_{BET} were estimated using Eq. (3):

$$S_{BET,total} = \frac{V_m N_s}{V} \text{ and } S_{BET} = \frac{S_{total}}{\alpha} \tag{3}$$

where N is Avogadro's number, s is the adsorption cross section of the adsorbing species, and α is the mass of adsorbent (g).

2.2.5. Proximate analysis

Moisture, ash, and volatile matter were analyzed by the method of the American Society for Testing and Materials Standard (ASTM standard –D1762–84). Approximately 1 g of biochar, sieved through a 2 mm mesh, was added into a porcelain crucible and the moisture content was calculated from the loss in weight at 105 °C in the oven for 2 h. After that, the crucibles used for moisture measurement were heated to 950 °C in a muffle furnace for a period of 6 min to measure volatile mater. Ash content was then calculated from the loss in weight of the samples contained in the crucibles (used for volatile matter) following heating at 750 °C for 6 h.

2.2.6. Elemental analysis (C, N, H)

5 mg of biochar, sieved through a 2 mm mesh, was loaded into a tin capsule and placed into an autosampler drum to remove any atmospheric nitrogen. The sample was then put into a vertical quartz tube and heated at 1000 °C with constant helium flow and pure oxygen in order to combust (oxidize) the sample completely. The gas mixture

containing the three components (C, N, H) from the oxidation step was separated via a chromatographic column and detected by a thermo-conductivity detector. The elemental analyzer used was a Carlo Erba EA1110 Model, Italy. The total O was calculated following the ASTM method as follows:

$$O\ (\%w/w) = 100 - ash\ (\%w/w) - C\ (\%w/w) - N\ (\%w/w) - H\ (\%w/w) \quad (4)$$

2.2.7. Total P, Ca, Mg, and K

Total P, Ca, Mg, K were measured after biochar (0.5 g) was put into a porcelain crucible heated to 500 °C over 2 h, and held at 500 °C for 8 h for dry combustion. The sample was then moved into the combustion vessel. Next, 5 mL HNO_3 was added to each vessel and the samples were digested by a heating block at 120 °C until dryness (5 h). The tubes were allowed to cool before adding 1.0 mL HNO_3 and 4.0 mL H_2O_2. After that, samples were preheated to 120 °C to dryness, and then dissolved with 1.43 mL HNO_3, made up with 18.57 mL deionized water to achieve 5% acid concentration, sonicated for 10 min, and filtered. The total P was measured by spectroscopy using a UV–Vis 2000 model with quartz cuvette at $\lambda = 725$ nm with 6 standards (0, 0.02, 0.04, 0.06, 0.08, 0.1 mg P_2O_5/100 mL) to establish the standard curve. Ca and Mg were titrated by EDTA (0.01 M) with murexide (the ammonium salt of purpuric acid) indicator for Ca and Eriochrome Black T for Mg. K was analyzed by Flame Atomic Adsorption Spectroscopy (FAAS 2900 model) with 4 standards (0.25, 0.5, 1.0, and 2.0 mg K/L).

2.2.8. Fourier-transform infrared (FTIR) spectroscopy

Approximately 0.5 g of biochar, sieved through a 2 mm mesh and dried at 60 °C, was used for FTIR analysis. The FTIR spectra of the biochar were measured using a Varian 660 spectrometer. The spectra were an average of 32 scans at 4 cm^{-1} scaning from 4000 to 400 cm^{-1}.

2.2.9. Statistical analysis

SPSS 22.0 software was used to conduct the statistical analysis of the data. All results are the mean of three replications with standard deviation displayed.

2.3. Biochar adsorption experiments

A stock solution (500 mg Zn^{2+}/L) was formed by dissolving Zn $(NO_3)_2.6H_2O$ in distilled water, and this was used to prepare the Zn^{2+} solutions for adsorption experiments with various Zn^{2+} and biochar concentrations. The experimental solutions were adjusted to pH 5.5 ± 0.2 by 0.1 M NaOH and/or 0.1 M HCl. The adsorption of Zn^{2+} onto the biochar was evaluated through methods modified from (Kołodyńska et al., 2012) with systematic variation of the initial concentrations of adsorbate (0.5 g biochar mixed with 40 mL of 0, 20, 40, 60, 80, 160, and 320 mg Zn^{2+}/L and shaken for 24 h), different dosages of adsorbent (0, 0.25, 0.5, 0.75, and 1.0 g of the BC mixed with 40 mL of 60 mg Zn^{2+}/L and shaken for 24 h), and different contact times (0.5 g biochar mixed with 40 mL of 60 mg Zn^{2+}/L and shaken for 30, 60, 90, 120, 150, 180, and 240 min). The suspensions were shaken on an orbital shaker at 300 rpm for the required durations at ambient temperature (20 ± 0.5 °C). At the specified time, the suspensions were centrifuged at 5000 rpm for 5 min and the supernatants filtered by acrodisc syringe filter (0.20 μm). The Zn^{2+} concentration in the filtered supernatant was measured by Flame Atomic Adsorption Spectrometry (Perkin Elmer AAnalyst 300 model) using a range of calibration standard concentrations (0, 0.25, 0.5, 1.0 and 2.0 ppm Zn^{2+}). All the experiments were conducted in triplicate. The Zn^{2+} adsorption onto biochar at equilibrium (q_e), at time t (q_t), and the percent of removal (%) were calculated using the equations presented below.

For equilibrium experiments:

$$q_e = \frac{(C_o - C_e)V}{m} \quad (5)$$

and

$$\%removal = \frac{C_o - C_e}{C_o} \times 100 \quad (6)$$

where C_o and C_e are the initial and equilibrium concentrations of Zn^{2+}; V (L) is the volume of the adsorbate (Zn^{2+} in this case); and m is the mass of adsorbent (biochar in this case) (g).

For the contact time experiments:

$$q_t = \frac{(C_o - C_t)V}{m} \quad (7)$$

and

$$\%removal = \frac{C_o - C_t}{C_o} \times 100 \quad (8)$$

where C_o (mg/L) and C_t (mg/L) are the initial and time t concentrations of Zn^{2+}; V (L) is the volume of the adsorbate solution; and m is the dosage of adsorbent (g).

2.3.1. Data analysis

The Langmuir isotherm and Freundlich isotherm models were used to evaluate the adsorption of Zn^{2+} onto the three biochar. Langmuir theory (Langmuir, 1917) assumes that adsorption of an adsorbate onto an adsorbent takes place as a homogenous surface monolayer (Cheng et al., 2008) with constant adsorption heat for all active sites and no interactions between the adsorbed molecules (Chowdhury et al., 2011). The model equation is as follows:

$$\frac{1}{q_e} = \frac{1}{q_{max}} + \frac{1}{q_{max} K_L} \frac{1}{C_e} \quad (9)$$

where q_e (mg/g) and q_{max} (mg/g) are the adsorption capacity of the adsorbent and the maximum monolayer adsorption capacity of the adsorbent in equilibrium, respectively; K_L (L/mg) is the Langmuir adsorption constant relating to the adsorption energy; and C_e (mg/L) is the concentration of the adsorbate at equilibrium.

Freundlich theory (Freundlich, 1906) assumes that the adsorbate molecules adsorb onto the adsorbent as a heterogeneous multilayer (Cheng et al., 2008) with unequal adsorption heats for the adsorption sites (Chowdhury et al., 2011). The equation is described as follows:

$$\ln q_e = \frac{1}{n} \ln C_e + \ln K_F \quad (10)$$

where q_e (mg/g) and C_e (mg/L) are the adsorption capacity of adsorbent and concentration of adsorbate at equilibrium, respectively; 1/n is the intensity of adsorption; and K_F (mg/g) is the Freundlich affinity coefficient.

2.3.2. Adsorption kinetics

The adsorption mechanism of porous adsorbents can be assessed by Pseudo-first order and Pseudo-second order models to understand the adsorption kinetics. The equations with linear form are shown, respectively as follows:

$$\ln(q_{e-exp} - q_t) = \ln q_{e-cal1} - k_1 t \quad (11)$$

and

$$\frac{t}{q_t} = \frac{1}{k_2 q_{e-cal2}^2} + \frac{t}{q_{e-cal2}} \quad (12)$$

where $q_{e\text{-}exp}$ (mg/g) is the experimentally obtained adsorption capacity of adsorbent at equilibrium; q_t (mg/g) is the amount of adsorbate adsorbed onto the biochar at time t (min); k_1 (min^{-1}) and k_2 (g/mg min) are the Pseudo-first order and Pseudo-second order rate constants, respectively; $q_{e\text{-}cal1}$ is calculated from plots of $\ln(q_{e\text{-}cal1}\text{-}q_t)$ versus t, while $q_{e\text{-}cal2}$ is obtained from plots of t/q_t versus t.

Table 1
Physico-chemical characteristics of the three biochar samples.

Parameters	Wood BC	Rice husk BC	Bamboo BC
pH	10.11 ± 0.04 a	9.51 ± 0.02 a	9.94 ± 0.02 a
CEC, Cmol/kg	13.53 ± 0.65 a	26.70 ± 1.57 c	20.77 ± 1.21 b
Moisture, %	5.45 ± 0.03 a	5.37 ± 0.05 a	6.11 ± 0.11 a
Volatile, %	46.68 ± 1.68 a	45.61 ± 0.54 a	48.72 ± 3.22 a
Ash, %	1.93 ± 0.03 a	41.24 ± 0.49 c	8.08 ± 0.20 b
Fixed carbon, %	45.94 ± 1.68 c	7.82 ± 0.10 a	37.09 ± 3.32 b
SA, m^2/g	479.34 ± 0.88c	434.53 ± 2.79b	3.29 ± 0.02a
C, %	82.10 ± 0.21 c	47.82 ± 0.18 a	80.27 ± 0.08 b
H, %	2.33 ± 0.01 a	2.07 ± 0.04 a	2.07 ± 0.04 a
N, %	0.71 ± 0.05 a	0.62 ± 0.06 a	0.72 ± 0.02 a
O, %	12.93 ± 0.16 a	8.25 ± 0.28 b	8.86 ± 0.02 b
P, %	0.22 ± 0.21 a	0.22 ± 0.20 a	0.88 ± 0.13 a
K, %	1.58 ± 0.62 a	1.89 ± 0.63 a	0.47 ± 0.13 a
Ca, %	0.65 ± 0.06 a	2.37 ± 0.18 b	0.57 ± 0.01 a
Mg, %	0.21 ± 0.05 a	0.26 ± 0.10 a	0.14 ± 0.03 a

Note: Data are mean values or ± standard deviation (duplicate for C, H, N, P, K, Ca, and Mg, and triplicate for pH, moisture, CEC, volatile mater, ash, fixed carbon, and BET surface area (SA)). The same letter indicates no significant difference ($p < 0.05$) while different letters indicate statistically significant differences between the BC samples.

2.3.3. Intraparticle diffusion model

The intraparticle diffusion model, based on the theory of (Weber and Morris, 1963), was used to evaluate the diffusion mechanisms of the porous adsorbents. The equation is given as:

$$q_t = k_{id} t^{1/2} + C \quad (13)$$

where k_{id} is the rate constant of the intraparticle diffusion (mg/g $min^{1/2}$), and C is the thickness of the boundary layer. C and k_{id} are calculated from the plot of q_t versus $t^{1/2}$.

3. Results and discussion

3.1. Physicochemical properties of biochar

The physicochemical properties of the three biochar used in this study are shown in Table 1, presented as mean ± SD (standard deviation). Results indicate that all three biochar were alkaline with similar pH values in the range 9.51–10.11 and high carbon contents (47.82 ± n0.18 to 82.10 ± 0.21%). The high pH values were caused by the separation of alkali salts from the organic matrix during the pyrolysis process (Chen et al., 2011) and then these salts were mixed in the ash. The alkali elements were analyzed including Ca, Mg and K, and these values were similar ($p > 0.05$), excepting Ca ($p < 0.05$).

The ash content shows significant differences ($p < 0.05$) among the biochar. The largest proportion of ash was found in the rice husk BC, with 41.24 (± 0.49) % ash, while the ash contents of wood and bamboo BC were 1.93 ± 0.03 and 8.08 ± 0.20%, respectively. The high ash content of rice husk BC (e.g., 54%) is consistent with previous reports (Shen et al., 2014), due to the biomass having lower abundance of lignin, e.g., 9–20% as compared to woody residues, e.g., 20–40%. However, the biochar with the highest ash content was found to correspond to lower values of fixed carbon (Yargicoglu et al., 2015). In fact, the fixed carbon of rice husk BC was only 7.82 ± 0.10%, compared to 45.94 ± 1.68% for bamboo BC. The low fixed carbon means that this material is less resistant to biotic decomposition and thus has a shorter existence in the environment (Yargicoglu et al., 2015).

The BET surface areas of the three biochar were significantly different ($p < 0.05$), as shown in Table 1, and correspond to the different morphologies and structures in the corresponding SEM images which indicate that wood and bamboo BCs have more porous structures than rice husk BC, which correlates with their higher BET surface area. Various shapes and sizes of pores were observed for wood and bamboo BC, while the morphology of rice husk shows elongated hollow regions (resembling the shape of a boat) with one side having a rough surface formed by mostly closed vesicles organised in rows, which were presumably formed by the melting of lignin while transporting the volatiles towards the surface (Sharma et al., 2002) and cracking and polymerization of hydrocarbons (Septien et al., 2013).

FTIR spectra of wood, rice husk, and bamboo BC were interpreted based on previous literature (Özçimen and Ersoy-Meriçboyu, 2010). The band at 2922 cm^{-1} of both bamboo and wood BC refers to the aliphatic C—H stretching of alkenes. The O—H stretching of carboxylic acids in the three BC is observed in the region of 2588–2532 cm^{-1}, while O—H and P—H stretching of ester compounds are assigned in the range of 2362–2348 cm^{-1}. The bands that appear at around 2160 cm^{-1} in rice husk and wood BC are attributed to aliphatic isonitrile –N ≡ C stretching, C═C stretching of alkynes, as well as Si—H stretching of silicon compounds.

The C═C stretching bands of aromatic compounds of the biochar appeared in the range 1587–1550 cm^{-1}, whereas aromatic C═C stretching and C—H bending bands are assigned between 875 cm^{-1} and 872 cm^{-1}. Interestingly, there was one band near 1430 cm^{-1} for rice husk BC only, suggesting silicon attachment to the ring of benzene. Bands in the range of Si-O-Si asymmetric stretching (1000–1130 cm^{-1}) were observed for both wood BC (1069 cm^{-1}) and rice husk BC (1058 cm^{-1}). In addition, CO_3^{2-} groups were also represented in the bands at 872 cm^{-1} for wood BC and bamboo BC or at 875 cm^{-1} for rice husk BC, while the bands appearing in the range of 950–1100 m^{-1} for wood BC (1069 m^{-1}) and rice husk BC (1058 m^{-1}) are assigned to PO_4^{3-} ions. In the range 1069–1058 cm^{-1}, C—O stretching bands of alcohols and phenols and aliphatic C—O stretching of esters were found in wood and rice husk BC, but were not present in bamboo BC. The bands observed between 803 and 796 cm^{-1} for all three biochar were associated with NH_2 wagging and twisting of amines, and aliphatic symmetric P–O–C stretching. Similarly, =C-H bending of alkynes and C—S stretching bands were identified in the range of 700–600 cm^{-1} and were present in all three biochar. Thus, the three biochar were dominated by an aromatic structure which result from the transformation of cellulose, hemicelluloses, and lignin and protein present in the parental feedstocks (Cantrell et al., 2012) to form condensed structures via aromatization (Harvey et al., 2011) during the pyrolysis process. This is consistent with the alkaline pH values measured for all three biochar. Additionally, carboxylic acid, alcohol, phenol, and amine functional groups were found to have formed on the biochar surfaces, which play an important role in cation and anion adsorption capacity of biochar, and indeed is consistent with the original biomass components.

There were significant differences in the CEC values among the three biochar ($p < 0.05$). In fact, rice husk BC had the highest CEC with 26.70 Cmol/kg, while bamboo and wood BC were 20.77 Cmol/kg and 13.53 Cmol/kg, respectively. A high CEC indicates the ability of biochar to adsorb cationic pollutants, such as Zn^{2+}. CEC depends on the presence of negatively charged surface functional groups and other sources like metal hydroxides and silica phytoliths in biochar ash (Harvey et al., 2011).

3.2. Effect of Zinc concentration on the adsorption capacity of biochar

The impact of different initial Zn^{2+} concentrations on adsorption ability and % Zn^{2+} removal by the biochar at a constant adsorbent value (12.5 g/L) is shown in Fig. 2. Zn^{2+} adsorption onto the three biochar increased as the initial Zn^{2+} concentration increased. In fact, there was a sharp increase in the adsorption for bamboo BC when the adsorbate concentrations rose from 40 mg/L to 80 mg/L, while this trend occurred for rice husk and wood BCs at Zn^{2+} concentration lower than 40 mg/L. The adsorption to the three biochar gradually decreased at higher metal concentrations (e.g., > 80 mg Zn^{2+}/L for bamboo BC or > 40 mg Zn^{2+}/L for both wood BC and rice husk BC). Interestingly, all three biochar had similar adsorption abilities when the Zn^{2+} concentrations were lower than 40 mg/L, while at the higher Zn^{2+}

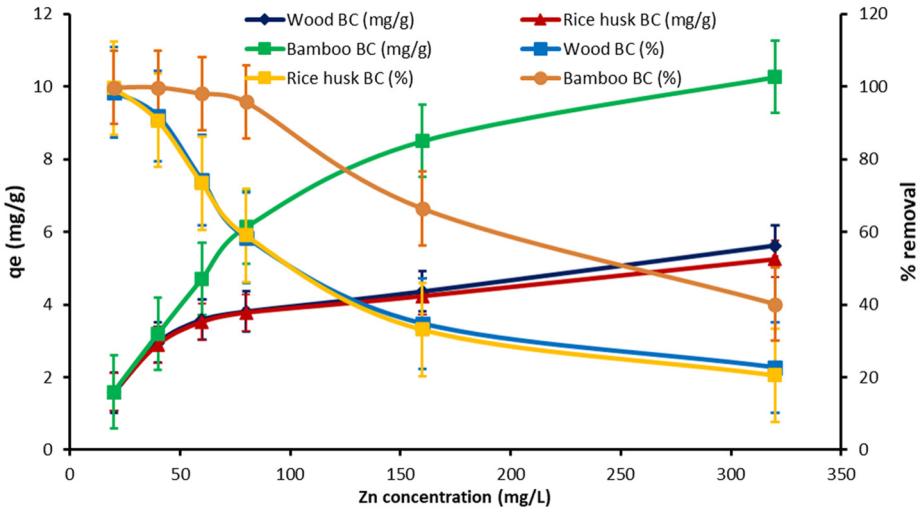

Fig. 2. Effect of initial adsorbate (Zn^{2+}) concentration on Zn^{2+} adsorption by biochar, where the biochar concentration was constant at 12.5 g/L, plotted as adsorption at equilibrium, q_e, (on the left y-axis) and as the proportion of initial Zn^{2+} removed (%) on the right y-axis. All experiments were performed in triplicate and data are presented as mean ± SD.

concentrations the adsorption capacity followed the order bamboo BC > wood BC ≈ rice husk BC.

The Zn^{2+} removal (%) by the biochar showed the opposite trend compared to the adsorption (see Fig. 2); although the % removals showed a dramatic decrease, the Zn^{2+} total (mg) removed by the biochar (12.5 g/L) increased with increased initial Zn^{2+} concentrations (see Table 2). For instance, when increasing the adsorbate concentration from 20 mg/L to 320 mg/L, the total amount of Zn^{2+} removed by both wood BC and rice husk BC was similar and increased from 19.76 ± 0.50 mg/L to 70.18 ± 3.40 mg/L. The increase in the total amount of Zn^{2+} removed also was observed for bamboo BC but with higher amounts, rising from 19.95 ± 0.02 mg/L to 128.30 ± 3.11 mg/L based on 12.5 g biochar. Thus, the fact that the bamboo BC was able to remove 40% of the initial Zn^{2+} at the highest concentration tested (320 mg/L) compared to just 20% being removed by the wood and rise husk BCs confirms the higher effectiveness of the bamboo BC for Zn^{2+} adsorption.

Interestingly, the biochar concentration of 12.5 g/L for both wood BC and rice husk BC could remove 99% of the Zn^{2+} in the solution containing 20 mg Zn^{2+}/L, while 90–92% removals were observed for the solution of 40 mg Zn^{2+}/L, which nearly meets the requirement for drinking water quality, this being < 3.0 mg Zn^{2+}/L (OECD, 2004), where the residual Zn^{2+} concentrations were 3.13 ± 0.07 mg/L for wood BC and 3.71 ± 0.25 mg/L for rice husk BC following incubation for 24 h. In contrast, bamboo BC (12.5 g/L) could remove > 98% of Zn^{2+} (the residual Zn^{2+} concentrations = 0.05 ± 0.02–1.16 ± 0.08 mg/L) from the 20 and 40 mg/L solutions, resulting in water that was fully compliant with the drinking water requirements, whereas 96% removal (residual Zn^{2+} concentration 3.37 ± 0.42 mg/L) was seen for the solution with initial concentration of 80 mg Zn^{2+}/L (see Fig. 2 & Table 2). Hence, bamboo BC is better able to remove Zn^{2+} at higher contamination levels than wood or rice husk BC.

3.3. Effect of biochar dosage on zinc adsorption

The results of Zn^{2+} ion adsorption onto the three biochar at various biochar masses were also investigated. The results indicate that increasing the concentration of biochar actually decreases the adsorption effectiveness of all three biochar for Zn^{2+} at the Zn^{2+} concentrations evaluated. These trends were similar to several previous reports, such as Chen et al. (2011) for hard wood and corn straw BC, Kołodyńska et al. (2012) for pig and cow manure BC or Pellera et al. (2012) for rice husk, olive pomance, orange waste, and compost BC (for Cu^{2+} adsorption). For example, when the adsorbent dosage increased four-fold from 6.25 g/L to 25 g/L, the Zn^{2+} adsorption onto wood BC and rice husk BC decreased by half from 4.06 ± 0.27 mg Zn^{2+}/g biochar to 2.06 ± 0.01 mg Zn^{2+}/g biochar, while the adsorption reduction of bamboo BC was even greater going from 6.97 ± 0.12 mg Zn^{2+}/g biochar to 2.35 ± 2.16 mg Zn^{2+}/g biochar.

The Zn^{2+} removal (%) increased with increasing adsorbent concentration. For instance, there was a sharp increase in Zn^{2+} removal for the three biochar when the adsorbent mass was increased from 6.25 g/L to 12.5 g/L. Beyond 12.5 g/L biochar, the % removal remained stable at around 98% for bamboo BC at biochar contents ≥12.5 g/L, while % removal by both wood BC and rice husk BC decreased gradually. These results indicated that the adsorbent dosage of 12.5 g/L was a turning point of adsorption for the biochar for 60 mg/L of adsorbate, and for this reason 12.5 g/L was chosen as the biochar dosage for the subsequent experiments in this study. Note however, that this would need to be reconfirmed if higher absorbate concentration solutions were to be remediated, e.g. wastewater sludge.

The adsorption mechanism of Zn^{2+} onto the biochar remains

Table 2
The mass of Zn^{2+} removed by biochar at the various initial Zn^{2+} concentrations.

Zn^{2+} initial Conc (mg/L)	Wood BC		Rice husk BC		Bamboo BC	
	C_e, mg/L	Removal, mg	C_e, mg/L	Removal, mg	Ce, mg/L	Removal, mg
20	0.24 ± 0.05	19.76 ± 0.05	0.07 ± 0.01	19.93 ± 0.01	0.05 ± 0.02	19.95 ± 0.02
40	3.13 ± 0.07	36.87 ± 0.07	3.71 ± 0.25	36.29 ± 0.25	0.08 ± 0.00	39.92 ± 0.00
60	15.23 ± 0.69	44.77 ± 0.69	15.91 ± 0.76	44.09 ± 0.76	1.16 ± 0.08	58.84 ± 0.08
80	32.43 ± 0.71	47.57 ± 0.71	32.75 ± 0.1.26	47.25 ± 1.26	3.37 ± 0.42	76.63 ± 0.42
160	105.55 ± 1.02	54.45 ± 1.02	107.04 ± 4.74	52.96 ± 4.74	53.74 ± 0.53	106.26 ± 0.53
320	249.82 ± 3.40	70.18 ± 3.40	254.38 ± 1.15	65.62 ± 1.15	191.70 ± 3.11	128.30 ± 3.11

Note: The biochar concentration was constant (12.5 g/L); C_e (mg/L) was the Zn^{2+} concentration in the filtered supernatant. The Zn^{2+} removal (mg) was calculated for 12.5 g biochar (total).

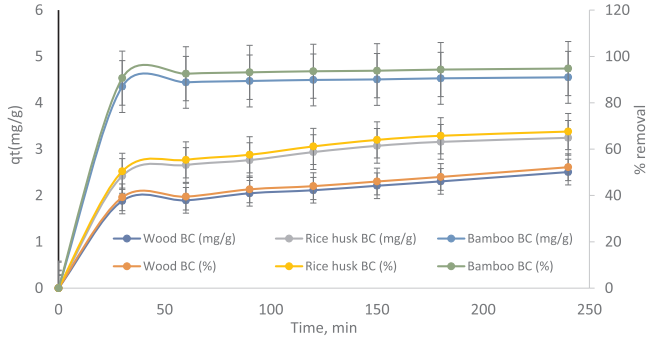

Fig. 3. Effect of contact time on biochar adsorption capacity, plotted as adsorption at time t, q_t, and as the proportion of initial Zn^{2+} removed (%). Adsorbent and adsorbate concentrations were 0.5 g and 60 mg/L, respectively, and data are based on three replicates presented as mean ± SD.

unclear. In fact, rice husk BC has the highest CEC (26.70 ± 1.57 Cmol/kg) and the lowest BET surface area (3.29 m^2), but had similar adsorption capacity as wood BC, even though the latter's CEC is much lower at 13.53 ± 0.65 Cmol/kg and BET surface area is much higher at 479.34 m^2. Additionally, the removal and adsorption capacity of all three biochar were similar when the biochar concentration reached 25 g/L. Further analysis of the data was thus performed to shed light on the adsorption mechanisms.

3.4. Effect of contact time on zinc adsorption by biochar

The effect of contact time on adsorption capacity and % removal of Zn^{2+} by the three biochar is presented in Fig. 3. The data showed that the adsorption capacity and removal of Zn^{2+} by the three biochar were quite different, and followed the order bamboo BC > rice husk BC > wood BC with increasing contact time. There was a fast adsorption for Bamboo BC in the first period (30 min) with 90.64 ± 1.75% of Zn^{2+} removed, and the removal increased slowly (an additional 4.15 ± 1.49%) after 240 min before reaching equilibrium.

In contrast, wood BC and rice husk BC both showed a more moderate removal, with the latter being the higher between the two. The removal of Zn^{2+} by rice husk BC in the first 30 min and after 240 min was 50.43 ± 7.01% and 67.59 ± 1.28%, respectively, while only 52.19 ± 1.28% of the adsorbate was removed over 240 min by wood BC. Thus, it could be concluded that the adsorption capacity depends not only on the adsorbents but also the adsorbate type, as different adsorption mechanisms are available.

3.5. Adsorption isotherms

The Langmuir and Freundlich Isotherm models are normally used to describe the relationship of the initial concentration of adsorbate (Zn^{2+}) in solution and the adsorbate content removed by the adsorbent (biochar) at equilibrium and at a certain temperature and pH. The Zn^{2+} adsorbed onto the biochar was analyzed to identify which model best describes (fits) the removal of adsorbate from solution onto the biochar surface: i.e., whether the adsorption results in monolayer or multilayer formation according to the theories of the two models. The Zn^{2+} adsorption isotherm was constructed using the data of the effect of initial concentration of Zn^{2+} which ranged from 20 mg/L to 320 mg/L on adsorption, as presented previously (Fig. 2). The fitting parameters obtained from the two models are shown in Table 3.

The parameters indicated that the Freundlich model (R^2 = 0.9668–0.9924) provides a better fit to the data than the Langmuir model (R^2 = 0.8981–0.9257), as indicated by the linear regression values. The q_{max} values of the Langmuir model, calculated from the plot of $1/q_e$ versus $1/C_e$ were also lower than the q_e values

Table 3
Langmuir and Freundlich constants derived from the data for Zn^{2+} adsorption onto the three biochar studied (wood, rice husk and bamboo).

Adsorbent	Langmuir model			Freundlich model		
	q_{max}	K_L	R^{2*}	K_F	1/n	R^{2**}
Wood BC	4.02	2.62	0.9257	2.17	0.16	0.9668
Rice husk BC	3.82	1.03	0.9030	2.35	0.14	0.9924
Bamboo BC	7.62	5.63	0.8981	4.73	0.15	0.9915

Note: q_{max}, K_L, and R^{2*} were obtained by plotting $1/q_e$ versus $1/C_e$ (Eq. (5)), while K_F, 1/n and R^{2**}were calculated from a plot of $\ln q_e$ versus $\ln C_e$ (Eq. (10)), respectively, using the data from Fig. 12.

from experiments (see Fig. 2). In addition, the heterogeneity coefficient (1/n) of the three biochar was in the range between 0 and 1, which indicated favourable adsorption (Radnia et al., 2011). This trend was also supported by Mubarak et al. (2013) for magnetic biochar, Doumer et al. (2016) for five biochar produced from sugarcane bagasse, eucalyptus forest residues, castor meal, green pericarp of coconut, and water hyacinth. However, these findings were opposite to several previous studies which supported a Langmuir model to explain the adsorption of the heavy metal (Zn^{2+}) to biochar, such as Chen et al. (2011) for hardwood BC (450 °C) and corn straw BC (600 °C), Kołodyńska et al. (2012) for pig and cow manure BCs (400 °C and 600 °C), Al-Wabel et al. (2013) for swithgrass and wood BC (500 °C), Frišták et al. (2015) for beech wood chip BC and garden waste green residue BC (500 °C). Thus, biochar produced from different biomasses and at various temperatures were found to have different adsorption capacities and adsorption mechanisms for zinc. In this study Zn^{2+} adsorption onto the three biochar was best fit using the Freundlich model, which means that the adsorption occurred as a heterogeneous surface multilayer.

3.6. Adsorption kinetics

The adsorption mechanism of the adsorbate (Zn^{2+}) by the biochar was evaluated through adsorption kinetics studies. Two kinetics models were investigated, a Pseudo-first order and a Pseudo-second order model. Both linear regression coefficients (R^2) and $q_{e\text{-}cal}$ values are normally used to assess the goodness of fit of kinetics models. The parameters obtained from the two models are shown in Table 4.

It can be seen that the pseudo first order model did not fit well to the experimental data (data from Fig. 3). This finding was proven by the $q_{e\text{-}cal}$ values (0.32–1.88 mg/g) which were observed to be much lower than the experimental values ($q_{e\text{-}exp}$ = 3.58–4.71 mg/g), and the linear regression coefficient values (R^2 = 0.9232–0.9885) were lower than those obtained from the pseudo second order model (R^2 = 0.9897–0.9998). In contrast, the values of $q_{e\text{-}cal}$ (2.64–4.58 mg/g) calculated from the pseudo second order model were similar to the experimental values, and the R^2 values were higher than those of the Pseudo first order model, particularly for bamboo BC (R^2 = 0.9998). The high correlation coefficients (≥0.9897) suggest that the Pseudo second order model could be applied for the entire adsorption process in all three biochar.

Furthermore, it could be concluded that the rate-limiting step of the adsorption of Zn^{2+} onto the biochar was controlled by chemical adsorption occurring on the heterogeneous biochar surface as a result of multilayer adsorption. These findings were also supported by Chen et al. (2011) for hard wood BC and corn straw BC, and by Mubarak et al. (2013) for magnetic biochar. Inner-sphere complexation, i.e., ions binding directly to the surface with no intervening water molecules, and precipitation were responsible for the Zn^{2+} adsorption to the biochar, while electrostatic-driven ion exchange played essentially no role in the adsorption process (Kołodyńska et al., 2012).

Han et al. (2013) reported heavy metal ion complexation with

Table 4
Rate parameters for the adsorption of Zn^{2+} onto the three biochar.

Adsorbent	Pseudo first order				Pseudo second order			Intraparticle diffusion		
	$q_{e\text{-}exp}$	$q_{e\text{-}cal}$	K_1	R^2	$q_{e\text{-}cal}$	K_2	R^2	K_{id}	C	R^2
Wood BC	3.58	1.88	0.002	0.9792	2.64	0.017	0.9897	0.064	1.46	0.9487
Rice husk BC	3.53	1.33	0.413	0.9885	3.45	0.016	0.9979	0.086	1.98	0.9834
Bamboo BC	4.71	0.32	0.003	0.9232	4.58	0.110	0.9998	0.019	4.28	0.9260

negatively charged surface functional groups (e.g. hydroxyl groups) and/or precipitation with PO_4^{3-} and CO_3^{2-} groups. All of these organic and inorganic groups were reported to be present in the three Vietnamese biochar studied here. The negligible adsorption of Zn^{2+} via electrostatic cation exchange was evidenced by rice husk BC which had the highest CEC (26.70 ± 1.57 Cmol/kg) in comparison with wood BC (13.53 ± 0.65 Cmol/kg) and bamboo BC (20.77 ± 1.21 Cmol/kg), but which had a similar adsorption capacity as wood BC (see Table 2). These findings were opposite to the adsorption behaviour of the same three biochar for NH_4^+-N, which was adsorbed in the order rice husk BC > bamboo BC > wood BC, indicating that depending on the nature of the pollutant to be remediated different biochar will be more or less suitable, subject to the mechanism of adsorption and the surface functionalization of the specific biochar. Clearly, adsorption via cation exchange was not the driving factor governing the adsorption of Zn^{2+} onto the three biochar studied here.

3.7. Intraparticle diffusion and adsorption mechanism

Intraparticle diffusion is normally investigated in order to understand the diffusion mechanism of an adsorbate onto a porous adsorbent like biochar. The transport of the adsorbate ions into the interior of biochar particles is called intraparticle diffusion (also known as internal diffusion by pore diffusion and/or surface diffusion). Thus, the Weber and Morris model (Eq. (13)) was used to simulate the adsorption process of Zn^{2+} ions onto the biochar, by plotting q_t versus $t^{1/2}$. If the plot is linear and passes through the origin, intraparticle diffusion is the sole rate limiting step in the adsorption process (Foo and Hameed, 2012). However, the plot did not pass through the origin (see Fig. 4), so the adsorption process of Zn^{2+} onto the biochar by intraparticle diffusion occurred in more than one step. The intraparticle diffusion of Zn^{2+} adsorbed onto the three biochar was presented in Fig. 4 and the model fitting parameters are shown in Table 4.

The initial increase (see Fig. 4) during the first 30 min (around 5.5 $min^{1/2}$) was a result of the diffusion of Zn^{2+} ions through the boundary layer (film) which surrounds the biochar particles, in order to reach the external surface of the biochar. After that, the pore diffusion and/or surface diffusion (intraparticle diffusion) of Zn^{2+} ions in the porous system of the biochar took place over 30–60 min (around 5.5–7.7 $min^{1/2}$) for bamboo BC, and over 30–150 min (around 5.5–13.4 $min^{1/2}$) for both rice husk and wood BCs. Worch (2012) reported that intraparticle diffusion mainly occurs in the macrospores (> 50 nm) and mesopores (2–50 nm) of biochar, whereas the micropore volume (< 2 nm) is attributed to adsorption (Rouquerol et al., 1994). The final steps in the Zn^{2+} absorption were observed to be the slowdown of the diffusion which occurred after 60 min (7.7 $min^{1/2}$) for bamboo BC, while after 150 min (7.7 $min^{1/2}$) for both rice husk and wood BCs. The decrease of the diffusion was caused by the low concentration of adsorbate in solution (Cheung et al., 2007) and the porous system (macrospores and mesopores) becoming filled by adsorbate. Hence, the diffusion of Zn^{2+} onto the various biochar depends not only on the structure of the adsorbent but also on the concentration of the adsorbate in the solution. In this case, bamboo BC had the biggest boundary layer (C_i = 4.28) and the lowest rate constant for intraparticle diffusion with k_i = 0.019 (see Table 4), but it had the highest adsorption capacity for Zn^{2+}. Thus, the increase of thickness of the boundary layer enhanced the driving force for the adsorption process.

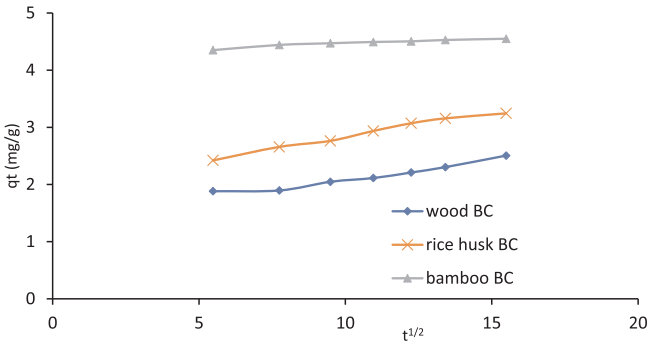

Fig. 4. Intraparticle diffusion plots for Zn^{2+} ions adsorbed onto the biochar. The value of q_t and the square root of t ($t^{1/2}$) were calculated using values from Fig. 3.

In summary, the adsorption of Zn^{2+} onto the three biochar particles occurred via intraparticle diffusion, complexation formation with organic surface groups, ion exchange, and precipitation with inorganic groups, as shown schematically in Fig. 5. The precipitation mainly occurred due to the alkaline pH of the biochar and was governed by both PO_4^{3-} and CO_3^{2-} groups for rice husk and wood BCs, while CO_3^{2-} groups participated for bamboo BC, which was determined from the FTIR data. The precipitation of Zn^{2+} with PO_4^{3-} and CO_3^{2-} groups was also reported previously (Han et al., 2013). Intraparticle diffusion and complexation also played an important role in the Zn^{2+} adsorption, while CEC was not a significant contributor to the Zn^{2+} adsorption for any of the biochar evaluated. Biochar from Vietnamese biomass including bamboo, woodchip and rice husk are thus a promising product with applications as a low cost and eco-friendly adsorbent for removing heavy-metal contaminants from aqueous solution.

4. Conclusion

The tested Vietnamese biomass residue–derived biochar effectively removed Zn^{2+} from aqueous solution. The Zn^{2+}-adsorption capacity of the biochar was bamboo BC > wood BC ~ rice husk BC, with bamboo BC (12.5 g/L) removing 96% of Zn^{2+} from aqueous solution containing 80 mg/L Zn^{2+}. Zn^{2+} adsorption fit the Freundlich model and thus occurred as a heterogeneous multilayer adsorption to the biochar surface, governed by chemical adsorption, and mainly based on complexation (organic groups) and precipitation (inorganic groups) rather than via cation exchange. Adsorption increased with increasing biochar concentration, while only bamboo BC also increased absorption with increasing adsorbate (Zn^{2+}) concentration.

CRediT authorship contribution statement

Nguyen Van Hien: Conceptualization, Investigation, Formal analysis, Visualization, Writing - original draft, Writing - review & editing, Funding acquisition. **Eugenia Valsami-Jones**: Supervision, Writing - review & editing. **Nguyen Cong Vinh**: Resources, Writing - review & editing. **Tong Thi Phu**: Resources, Writing - review &

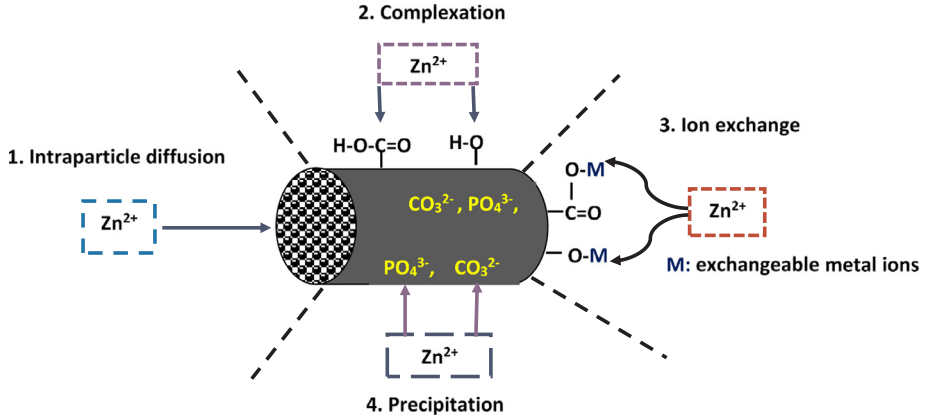

Fig. 5. Schematic of the mechanisms of Zn^{2+} adsorption onto each of the three biochar.

editing. **Nguyen Thi Thanh Tam:** Resources, Writing - review & editing. **Iseult Lynch:** Conceptualization, Methodology, Writing - original draft, Writing - review & editing, Supervision, Funding acquisition.

Acknowledgements

The authors would like to thank the Vietnamese government for funding via the Ministry of Agriculture and Rural Development (MARD) and the Vietnam International Education Development (VIED) - Ministry of Education and Training, known as "The priority programme of development and application of biotechnology to agriculture and rural development up to 2020" (Grant Agreement No 11/2006//QĐ -TTg). Additional support and funding for the project came from EU FP7 Marie Curie Career Integration Grant EcofriendlyNano (Grant Agreement no. PCIG14-GA-2013-631612). The authors acknowledge excellent technical support from Dr. Maria Thompson (University of Birmingham, UK) and Le Xuan Anh (Soils and Fertilizers Research Institute, Vietnam).

Data availability

Raw data are available upon request.

Declaration of competing interest

The authors declare that they have no known competing financial interests or personal relationships that could have appeared to influence the work reported in this paper.

Appendix A. Supplementary data

Fig. S1 – BET; Fig. S2 - SEM images of the three biochar samples; Fig. S3. FTIR spectra of wood, rice husk, and bamboo BC samples; Fig. S4 – Pseudo first order model did not fit well to the experimental data in Fig. 3 (adsorption time versus adsorption amount); Fig. S5 – Plot for a Pseudo-second order model fit to the data in Fig. 3 (adsorption time versus adsorption amount). Supplementary data to this article can be found online at https://doi.org/10.1016/j.biteb.2020.100466.

References

Al-Wabel, M.I., Al-Omran, A., El-Naggar, A.H., Nadeem, M., Usman, A.R., 2013. Pyrolysis temperature induced changes in characteristics and chemical composition of biochar produced from conocarpus wastes. Bioresour. Technol. 131, 374–379.
Beesley, L., Marmiroli, M., 2011. The immobilisation and retention of soluble arsenic, cadmium and zinc by biochar. Environ. Pollut. 159, 474–480.
Brunauer, S., Emmett, P.H., Teller, E., 1938. Adsorption of gases in multimolecular layers. J. Am. Chem. Soc. 60, 309–319.
Cantrell, K.B., Hunt, P.G., Uchimiya, M., Novak, J.M., Ro, K.S., 2012. Impact of pyrolysis temperature and manure source on physicochemical characteristics of biochar. Bioresour. Technol. 107, 419–428.
Chen, X., Chen, G., Chen, L., Chen, Y., Lehmann, J., McBride, M.B., Hay, A.G., 2011. Adsorption of copper and zinc by biochars produced from pyrolysis of hardwood and corn straw in aqueous solution. Bioresour. Technol. 102, 8877–8884.
Cheng, C.-H., Lehmann, J., Engelhard, M.H., 2008. Natural oxidation of black carbon in soils: changes in molecular form and surface charge along a climosequence. Geochim. Cosmochim. Acta 72, 1598–1610.
Cheung, W., Szeto, Y., McKay, G., 2007. Intraparticle diffusion processes during acid dye adsorption onto chitosan. Bioresour. Technol. 98, 2897–2904.
Chowdhury, Z.Z., Zain, S.M., Rashid, A., Khalid, K., 2011. Linear regression analysis for kinetics and isotherm studies of sorption of manganese (II) ions onto activated palm ash from waste water. Orient. J. Chem. 27, 405–415.
Dali-Youcef, N., Ouddan, B., Derriche, Z., 2006. Adsorption of zinc on natural sediment of Tafna River (Algeria). J. Hazard. Mater. 137, 1263–1270.
Demirbas, A., 2004. Effects of temperature and particle size on bio-char yield from pyrolysis of agricultural residues. J. Anal. Appl. Pyrolysis 72, 243–248.
Doula, M.K., 2009. Simultaneous removal of Cu, Mn and Zn from drinking water with the use of clinoptilolite and its Fe-modified form. Water Res. 43, 3659–3672.
Doumer, M., Rigol, A., Vidal, M., Mangrich, A., 2016. Removal of Cd, Cu, Pb, and Zn from aqueous solutions by biochars. Environ. Sci. Pollut. Res. 23, 2684–2692.
Foo, K., Hameed, B., 2012. Textural porosity, surface chemistry and adsorptive properties of durian shell derived activated carbon prepared by microwave assisted NaOH activation. Chem. Eng. J. 187, 53–62.
Freundlich, H., 1906. Over the adsorption in solution. J. Phys. Chem. 57, 1100–1107.
Frišták, V., Pipíška, M., Lesný, J., Soja, G., Friesl-Hanl, W., Packová, A., 2015. Utilization of biochar sorbents for Cd2+, Zn2+, and Cu2+ ions separation from aqueous solutions: comparative study. Environ. Monit. Assess. 187, 4093.
Gaskin, J., Steiner, C., Harris, K., Das, K., Bibens, B., 2008. Effect of low-temperature pyrolysis conditions on biochar for agricultural use. Trans. ASABE 51, 2061–2069.
González-Muñoz, M.J., Rodríguez, M.A., Luque, S., Álvarez, J.R., 2006. Recovery of heavy metals from metal industry waste waters by chemical precipitation and nanofiltration. Desalination 200, 742–744.
Han, Y., Boateng, A.A., Qi, P.X., Lima, I.M., Chang, J., 2013. Heavy metal and phenol adsorptive properties of biochars from pyrolyzed switchgrass and woody biomass in correlation with surface properties. J. Env. M Environ. Manage 118, 196–204.
Harvey, O.R., Herbert, B.E., Rhue, R.D., Kuo, L.-J., 2011. Metal interactions at the biochar-water interface: energetics and structure-sorption relationships elucidated by flow adsorption microcalorimetry. Environ. Sci. Technol. 45, 5550–5556.
Joseph, S., Taylor, P., 2014. The production and application of biochar in soils. In: Advances in Biorefineries. Elsevier, pp. 525–555.
Joseph, S., Camps-Arbestain, M., Lin, Y., Munroe, P., Chia, C., Hook, J., Van Zwieten, L., Kimber, S., Cowie, A., Singh, B., 2010. An investigation into the reactions of biochar in soil. Soil Res. 48, 501–515.
Kabata-Pendias, A., 2010. Trace Elements in Soils and Plants. CRC Press.
Kabbani, A., Karnib, M., Holail, H., Olama, Z., 2014. Heavy metals removal using activated carbon, silica and silica activated carbon composite. Energy Procedia 50, 113–120.
Kołodyńska, D., Wnętrzak, R., Leahy, J., Hayes, M., Kwapiński, W., Hubicki, Z., 2012. Kinetic and adsorptive characterization of biochar in metal ions removal. Chem. Eng. J. 197, 295–305.
Langmuir, I., 1917. The constitution and fundamental properties of solids and liquids. J. Franklin I 183, 102–105.
Lu, C., Chiu, H., 2006. Adsorption of zinc (II) from water with purified carbon nanotubes. Chem. Eng. Sci. 61, 1138–1145.
Méndez, A., Tarquis, A.M., Saa-Requejo, A., Guerrero, F., Gascó, G., 2013. Influence of pyrolysis temperature on composted sewage sludge biochar priming effect in a loamy soil. Chemosphere 93, 668–676.
Moreno-Barbosa, J.J.L.-V., Catalina, Maldonado, Andrea del Pilar, Giraldo, Liliana, Moreno-Piraján, Juan Carlos, 2013. Removal of lead(II) and zinc(II) ions from aqueous solutions by adsorption onto activated carbon synthesized from watermelon shell and walnut shell. Adsorption 19, 675–685.

Mubarak, N., Alicia, R., Abdullah, E., Sahu, J., Haslija, A.A., Tan, J., 2013. Statistical optimization and kinetic studies on removal of Zn 2+ using functionalized carbon nanotubes and magnetic biochar. J. Environ. Chem. Eng. 1, 486–495.
Mukherjee, A., Zimmerman, A.R., 2013. Organic carbon and nutrient release from a range of laboratory-produced biochars and biochar–soil mixtures. Geoderma 193, 122–130.
Mukherjee, A., Zimmerman, A., Harris, W., 2011. Surface chemistry variations among a series of laboratory-produced biochars. Geoderma 163, 247–255.
Özçimen, D., Ersoy-Meriçboyu, A., 2010. Characterization of biochar and bio-oil samples obtained from carbonization of various biomass materials. Renew. Energy 35, 1319–1324.
Pellera, F.-M., Giannis, A., Kalderis, D., Anastasiadou, K., Stegmann, R., Wang, J.-Y., Gidarakos, E., 2012. Adsorption of Cu (II) ions from aqueous solutions on biochars prepared from agricultural by-products. J. Environ. Manag. 96, 35–42.
Qiu, Y., Zheng, Z., Zhou, Z., Sheng, G.D., 2009. Effectiveness and mechanisms of dye adsorption on a straw-based biochar. Bioresour. Technol. 100, 5348–5351.
Radnia, H., Ghoreyshi, A.A., Younesi, H., 2011. Isotherm and kinetics of Fe (II) adsorption onto chitosan in a batch process. IJEE 2, 250–257.
Rajkovich, S., Enders, A., Hanley, K., Hyland, C., Zimmerman, A.R., Lehmann, J., 2012. Corn growth and nitrogen nutrition after additions of biochars with varying properties to a temperate soil. Biol. Fertil. Soils 48, 271–284.
Rouquerol, J., Avnir, D., Fairbridge, C., Everett, D., Haynes, J., Pernicone, N., Ramsay, J., Sing, K., Unger, K., 1994. Recommendations for the characterization of porous solids (Technical Report). Pure Appl. Chem. 66, 1739–1758.
Samper, E., Rodríguez, M., De la Rubia, M., Prats, D., 2009. Removal of metal ions at low concentration by micellar-enhanced ultrafiltration (MEUF) using sodium dodecyl sulfate (SDS) and linear alkylbenzene sulfonate (LAS). Sep. Purif. Technol. 65, 337–342.
Septien, S., Valin, S., Peyrot, M., Spindler, B., Salvador, S., 2013. Influence of steam on gasification of millimetric wood particles in a drop tube reactor: experiments and modelling. Fuel 103, 1080–1089.
Sharma, R.K., Wooten, J.B., Baliga, V.L., Martoglio-Smith, P.A., Hajaligol, M.R., 2002. Characterization of char from the pyrolysis of tobacco. J. Agric. Food Chem. 50, 771–783.
Shen, Y., Zhao, P., Shao, Q., 2014. Porous silica and carbon derived materials from rice husk pyrolysis char. Microporous Mesoporous Mater. 188, 46–76.
Sohi, S., Lopez-Capel, E., Krull, E., Bol, R., 2009. Biochar, climate change and soil: a review to guide future research. CSIRO Land and Water Science Report 5, 17–31.
Song, W., Guo, M., 2012. Quality variations of poultry litter biochar generated at different pyrolysis temperatures. J. Anal. Appl. Pyrolysis 94, 138–145.
Uchimiya, M., Wartelle, L.H., Klasson, K.T., Fortier, C.A., Lima, I.M., 2011. Influence of pyrolysis temperature on biochar property and function as a heavy metal sorbent in soil. J. Agric. Food Chem. 59, 2501–2510.
Vinh, N., Hien, N., Anh, M., Lehmann, J., Joseph, S., 2014. Biochar treatment and its effects on rice and vegetable yields in mountainous areas of northern Vietnam. IJASS 2, 5–13.
Weber, W.J., Morris, J.C., 1963. Kinetics of adsorption on carbon from solution. J. Sanit. Eng. Div. ASCE 89, 31–60.
WHO (World Health Organization), 2004. Guidelines for Drinking-Water Quality.
Worch, E., 2012. Adsorption Technology in Water Treatment: Fundamentals, Processes, and Modeling. Walter de Gruyter.
Yargicoglu, E.N., Sadasivam, B.Y., Reddy, K.R., Spokas, K., 2015. Physical and chemical characterization of waste wood derived biochars. Waste Manag. 36, 256–268.
Zheng, W., Guo, M., Chow, T., Bennett, D.N., Rajagopalan, N., 2010. Sorption properties of greenwaste biochar for two triazine pesticides. J. Hazard. Mater. 181, 121–126.